HHS Public Access

Author manuscript

Adv Healthc Mater. Author manuscript; available in PMC 2024 July 01.

Published in final edited form as:

Adv Healthc Mater. 2023 July ; 12(19): e2203209. doi:10.1002/adhm.202203209.

Outersphere Approach to Increasing the Persistance of Oxygen-Sensitive Europium(II)-Containing Contrast Agents for Magnetic Resonance Imaging with Perfluorocarbon Nanoemulsions toward Imaging of Hypoxia

Jacob C. Lutter[‡],
Department of Chemistry, Wayne State University, 5101 Cass Avenue, Detroit, Michigan 48202, USA

Andrea L. Batchev[‡],
Department of Chemistry, Wayne State University, 5101 Cass Avenue, Detroit, Michigan 48202, USA

Caitlyn J. Ortiz,
Department of Integrative Physiology, Baylor College of Medicine, Houston, TX 77030, USA

Alexander G. Sertage,
Department of Chemistry, Wayne State University, 5101 Cass Avenue, Detroit, Michigan 48202, USA

Jonathan Romero,
Department of Integrative Physiology, Baylor College of Medicine, Houston, TX 77030, USA

S. A. Amali S. Subasinghe,
Department of Chemistry, Wayne State University, 5101 Cass Avenue, Detroit, Michigan 48202, USA

Steen E. Pedersen,
Department of Integrative Physiology, Baylor College of Medicine, Houston, TX 77030, USA

Md Abul Hassan Samee,
Department of Integrative Physiology, Baylor College of Medicine, Houston, TX 77030, USA

Robia G. Pautler,
Department of Integrative Physiology, Baylor College of Medicine, Houston, TX 77030, USA

Matthew J. Allen
Department of Chemistry, Wayne State University, 5101 Cass Avenue, Detroit, Michigan 48202, USA

mallen@chem.wayne.edu, rpautler@bcm.edu.
Present Address: J. C. Lutter, Department of Chemistry and Biochemistry, University of Southern Indiana, Evansville, IN 47712, USA
[‡]These authors contributed equally to this work.

Supporting Information
Supporting Information is available from the Wiley Online Library or from the author.

Abstract

Radiographic mapping of hypoxia is needed to study a wide range of diseases. Complexes of Eu^{II} are a promising class of molecules to fit this need, but they are generally limited by their rapid oxidation rates in vivo. Here, a perfluorocarbon-nanoemulsion perfused with N_2, forms an interface with aqueous layers to hinder oxidation of a new perfluorocarbon-soluble complex of Eu^{II}. Conversion of the perfluorocarbon solution of Eu^{II} into nanoemulsions results in observable differences between reduced and oxidized forms by MRI both in vitro and in vivo. Oxidation in vivo occurrs over a period of ~30 min compared to <5 min for a comparable Eu^{II}-containing complex without nanoparticle interfaces. These results represent a critical step toward delivery of Eu^{II}-containing complexes in vivo for the study of hypoxia.

Graphical Abstract

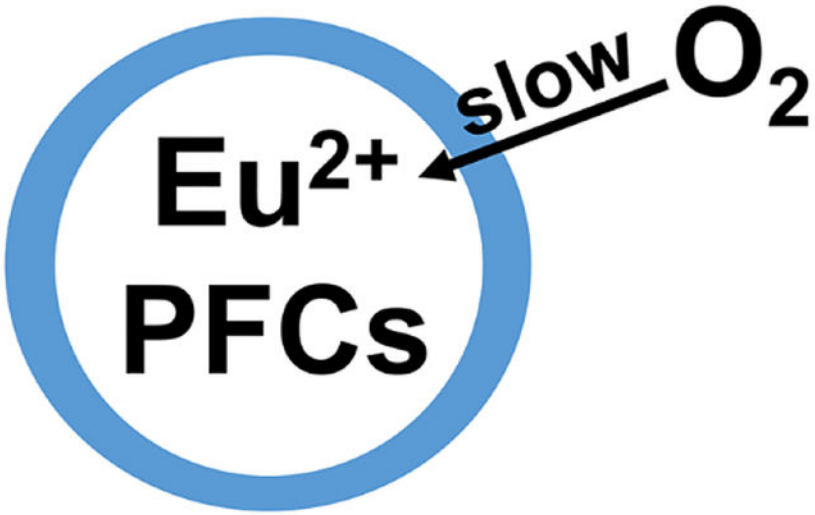

A new Eu(II) complex containing 44 fluorine atoms enables dispersion of the metal in de-oxygenated perfluorocarbon nanoemulsions to hinder the outersphere approach of oxygen to the metal. The nanoemulsion system increases the persistance of Eu(II) in vivo as observed by changs in ^{19}F-magnetic resonance imaging.

Keywords

Eu^{II}; hypoxia; MRI; perfluorocarbons

1. Introduction

The ability to image the presence or absence of oxygen in living systems is of paramount importance to the study of biochemistry, medicine, and several diseases. For example, hypoxia is a condition in which the amount of molecular oxygen is abnormally low and is correlated with diseases including several aggressive forms of cancer.[1] Consequently, there has been significant research effort toward monitoring oxygen content in vivo.[2] One promising route to examine hypoxia involves the use of probes for magnetic resonance

imaging (MRI), including metals that change oxidation state in the presence of O_2 resulting in a change in the ability to influence contrast with this imaging modality.[3] Specifically, the $Eu^{II/III}$ couple is accessible within biological systems. More specifically, Eu^{II} shortens T_1 relaxation times of water protons but is readily oxidized by O_2 to non-T_1-shortening Eu^{III}.[4] The oxidation states of Eu have marked differences in spectroscopic, electronic, and magnetic properties that enable this facile discrimination.[5] Therefore, these properties have been leveraged within MRI to explore the imaging of hypoxia.[3g,6] The greatest challenge toward using Eu^{II} for in-vivo imaging is its irreversible, rapid oxidation to Eu^{III} by O_2. For decades, research into tuning the oxidative stability of Eu^{II}-containing complexes focused on thermodynamic approaches through modifying coordination chemistry that enable complexes of Eu^{II} to be used for imaging low-oxygen environments upon direct injection into sites of interest.[3g,6,7] A major obstacle of responsive contrast agents, however, is the deconvolution of alterations in signal due to the desired stimulus compared to diffusion.[8] A promising research direction is the use of multimodal imaging approaches for ratiometric imaging where changes in two modes of relaxation negates the need to know the concentration of a single agent. The $Eu^{II/III}$ redox couple has been used with such systems involving ^{1}H-MRI, ^{19}F-MRI, and chemical exchange saturation transfer imaging,[5a,6a,9] but these approaches often take longer than the half-life of Eu^{II} in normoxic environments, requiring direct injection into sites of interest. To push beyond the limits of stabilizing complexes through thermodynamics, we sought kinetic approaches to slow the oxidation of Eu^{II} to enable its persistence long enough for ratiometric imaging, a critical step for enabling systemic delivery of Eu^{II} for the study of a wide range of diseases not accessible with direct injection. Along those lines, we recently reported the first Eu^{II}-containing complex that persists in oxygenated solution based on *innersphere* kinetics through the use of a phosphonate cage that regulates access to the innersphere of Eu^{II}.[10] Here, we report an approach that extends the persistence of Eu^{II} solubilized in a perfluorocarbon nanoemulsion by regulating access of oxygen into the *outersphere* environment of Eu^{II} by creating an oxygen-free outersphere encapsulated by interfaces (Figure 1).

We hypothesized that dispersing Eu^{II} in O_2-free perfluorocarbon nanoemulsions would create interfaces to slow the approach of solubilized O_2 through the outersphere environment of Eu^{II}, and consequently, slow the oxidation of Eu^{II} to Eu^{III}. Membranes are known to slow the diffusion of gasses, and specifically lecithin layers are known to decrease the rate of oxygen transport across interfaces.[11] Oxygen diffusion through perfluorocarbon interfaces is also reliant on a partial pressure gradient of gasses. Therefore, we hypothesized that interfaces created by a layer of lecithin surrounding perfluorocarbons saturated with the inert gas N_2 would slow the diffusion of oxygen into the outersphere environment of Eu^{II}-containing complexes. Furthermore, perfluorocarbons are chemically inert, have a rich history of in-vivo applications,[12] provide a source of fluorine that can be imaged via ^{19}F-MRI without background signal in vivo.[13] Finally, we previously showed the ^{19}F-MRI signal of nearby ^{19}F-nuclei is attenuated by Eu^{II} line-broadening properties and ameliorated by oxidation to Eu^{III}.[6a] Therefore, we hypothesized that a lecithin–deoxygenated-perfluorocarbon interface would interfere with the approach of oxygen toward Eu^{II} within the deoxygenated perfluorocarbon, thereby prolonging the persistence of Eu^{II} in normoxic tissue relative to Eu^{II}-containing complexes outside of the nanoemulsions.

Nanoemulsions of the perfluorocarbons are needed to enable compatibility with in-vivo injection due to the hydrophobic and lipophobic nature of perfluorocarbons. We also posited that the oxidation of Eu^{II} to Eu^{III} could be monitored using ^{19}F-MRI because ^{19}F-signal of the perfluorocarbon emulsion would increasingly appear with increasing concentrations of Eu^{III} as the line-broadening effects of Eu^{II} diminish with its oxidation.

2. Results and Discussion

2.1. Synthesis of Eu^{II}-containing Perfluorocarbons

To synthesize a compound that is both Eu-containing and perfluorocarbon soluble, we sought a tetra-amide cyclen derivative that contains linear alkyl perfluorinated arms. Historically, such ligands are straightforward to design and have the ability to bind lanthanide ions tightly, including Eu^{II} and Eu^{III}.[3a,6a,14] Thus, we synthesized the complex {europium(III)[(*N*,*N*',*N*'',*N*'''-tetra(*N*-(1H,1H-undecafluorohexyl)acetamidyl)-1,4,7,10-tetraazacyclododecane]} (Eu1) tris(trifluoromethanesulfonate) tetrahydrate to coordinate Eu^{III} and contain enough ^{19}F atoms to solubilize the complex in perfluorocarbons.

One commonly employed perfluorocarbon in medicine is *n*-perfluorooctylbromide (PFOB) thanks to its low water and lipid solubility and long clearance time in vivo.[13g] However, **Eu1** is not soluble in PFOB, but the inclusion of a minimal amount of a more polar compound, 1H,1H-perfluorooctylalcohol (PFOA, 20% *w*/*w*) afforded solubility of the complex. **Eu1** and its Eu^{II} reduction product (**Eu2**) are both soluble in the mixture of PFOA and PFOB but are insoluble in water. Reduction of Eu^{III} to Eu^{II} using zinc dust in the PFOA/PFOB solution was confirmed using UV–visible absorption, luminescence, and EPR spectroscopies (Figures S14–S16, Supporting Information). Finally, to determine the effect of oxidation of Eu^{II} to Eu^{III} from the diffusion of oxygen into the perfluorocarbon solution, we compared ^{19}F-NMR spectra of equimolar (4.5 mM) concentrations of **Eu1** and **Eu2** in degassed and aerated perfluorocarbons (Figures 2, S20, and S21). A change of roughly 29% in signal intensity was observed between degassed solutions of **Eu1** and **Eu2**, and that difference was more than an order of magnitude greater than the difference between aerated and degassed solutions of **Eu1**. These results demonstrate that oxidation of Eu^{II} to Eu^{III}, and not solely the presence of O_2, is the main cause of the increase in ^{19}F-MRI.

2.2 Eu2 in a mixture of perfluorocarbons is resilient to ambient oxidation when interfaced with non-degassed water

The resilience to oxidation of the solution of **Eu2** in PFOA/PFOB was examined using UV–visible absorption spectroscopy and ambient atmosphere, which is representative of the amount of oxygen in the lungs. Here, the pO_2 ranges from 0 mmHg in the de-oxygenated mixture atmospheric (~160 mmHg) in the sample exposed to air. The absorbance of the 4f–5d band at 350 nm was monitored over time for the conversion of Eu^{II} to Eu^{III}. Direct exposure of a solution of **Eu2** to the atmosphere yielded conversion to a solution of **Eu1** within ten minutes. These data demonstrate that the $Eu^{II/III}$ redox couple is accessible with the complex dissolved in the perfluorocarbon. However, the addition of a layer of nondegassed deionized water between the **Eu2** solution and ambient atmosphere, to simulate

injection into blood, led to no sign of oxidation after 120 minutes (Figure 3). These data suggest that the immiscibility of the perfluorocarbon in water protects Eu^{II} from ambient oxidation.

2.3 Eu2 in a perfluorocarbon nanoemulsion can be ratiometrically scaled to a ^{19}F signal in vitro

Solutions of **Eu1** or **Eu2** in PFOA/PFOB were converted into nanoemulsions in phosphate-buffered saline (1×) using the phospholipid lecithin to coat the surface of each nanoemulsion bubble. These emulsions were created under an atmosphere of N_2 to enforce the presence of inert gas in the perfluorocarbon solution to slow the diffusion of O_2 through the interface. Average particle size was determined using a microfluidic instrument to be 199 ± 31 nm in diameter (Figure S17, Supporting Information). To understand the relationship of **Eu1** vs **Eu2** content in the perfluorocarbon emulsion, chemical-shift imaging was performed on samples containing controlled ratios of **Eu1**/**Eu2** that were prepared in the absence of O_2 (Figure 4). The data shows a trend of decreasing signal as the percentage of **Eu2** increases, although the difference in signal intensity between 50 and 75% **Eu2** was not statistically significant (Figure S18). We studied ^{19}F signal because the perfluorocarbon nanoemulsions containing **Eu1** or **Eu2** did not differentially change the relaxation rate of water. Chemical-shift imaging was used to measure the ^{19}F signal, as opposed to the measuring the collective ^{19}F signal, to enable spatial mapping in the future due to the shorter imaging times needed to image a single resonance compared to all of the resonances that span >60 ppm (Figures S20 and S21).[15] In these imaging experiments, the ^{19}F signal of the perfluorocarbons of the emulsion (Figure S19) were used for chemical-shift imaging, as opposed to signals from the ligand, because of the ~700× greater concentration of the emulsion perfluorocarbons relative to the ligand. Further, the peak with the largest response to oxidation of Eu^{II} to Eu^{III} was the selected peak. In essence, the hydrophobic perfluorocarbon chains on the ligand enable solubility in perfluorocarbon emulsions and were not directly imaged in our studies. In general, when the content of **Eu2** increases, signal intensity from the perfluorocarbon emulsion decreases, due to line-broadening of ^{19}F signal by Eu^{II}, and therefore, the difference in ^{19}F signal intensity was measured as opposed to a difference in chemical shift. These results indicate that detection of the Eu-based redox event is possible using ^{19}F-MRI and that signal intensity correlates with the ratio of Eu^{II} to Eu^{III}.

2.4 ^{19}F Eu2 in a perfluorocarbon nanoemulsion extends the persistence of Eu^{II} in vivo

Given these promising initial results, the emulsions prepared in the absence of O_2 with **Eu2** (0.37 mM) were injected into the thigh muscle of mice to study the possibility for in vivo application. We chose intramuscular injections to enable comparison with a control Eu^{II}-containing complex, {europium(II) [(*N,N',N'',N'''*-tetra(*N*-(4-trifluoromethylphenyl)acetamidyl)-1,4,7,10-tetraazacyclododecane]}bis-chloride (**12F**), that is not in pefluorocarbon nanoparticles. The discrete complex was chosen to enable head-to-head comparison of Eu^{II}-containing complexes inside and outside perfluorocarbon nanoemulsions beause **Eu2** is not water-soluble. The discrete molecule **12F** enhances the relaxation rate of water protons observed with ^{1}H-MRI,[6a] and **Eu2**

in the perfluorocarbon nanoemulsion influences the ^{19}F signal from the perfluorocarbons. Therefore, a decrease of ^{1}H-MRI for **12F** and an increase of ^{19}F-MRI for **Eu2** directly inform on the oxidation of Eu^{II} to Eu^{III} caused by O_2. Because the control complex is expected to have a different rate of diffusion than a nanoparticle, we selected an injection route that minimizes diffusion, so that changes in signal could be attributed to oxidation of Eu^{II} to Eu^{III}. ^{1}H-MRI signal intensity of water in the presence of **12F** (6 mM in 3-morpholinopropane-1-sulfonic acid buffer, pH 7.4, 200 μL) and ^{19}F-MRI signal intensity for nanoemulsions of **Eu2** (0.37 mM of Eu, 200 μL) were monitored over time after intramuscular injection (Figure 5). ^{1}H-MRI data demonstrate a rapid decrease in signal over the first 5 minutes for **12F**, consistent with oxidation of Eu^{II} to Eu^{III} caused by O_2, similar to previous reports.[3g,4,6] However, a slower change over 30 minutes was observed with the ^{19}F-MRI signal from the emulsion. This trend is consistent with the oxidation of **Eu2** to **Eu1** over time as O_2 diffuses into the nanoparticle across the interfaces to oxidize Eu^{II} to Eu^{III}. The hydrophobic nature of **Eu1** and **Eu2** and the thermodynamic stability of $Eu^{II/III}$ in tetra-amide derivatives of cyclen further support changes in ^{19}F signal intensity as attributable to Eu^{II} oxidation to Eu^{III} because leakage of **Eu2** from the perfluorocarbon nanoemulsion and decomplexation of $Eu^{II/III}$ are unlikely.[5a,16] The shorter persistence in vivo than in the interface study in Figure 3 are likely due to the increased ratio of surface area to volume for nanoemulsions compared to bulk samples as well as increased mixing of nanoemulsions with the environment in vivo compared to in a cuvette because both surface area and mixing are known to influence diffusion across interfaces. Overall, from these experiments, we conclude that the emulsion is extending the persistence of Eu^{II} in vivo compared to a water-soluble agent.

3. Conclusions

Eu^{II}-containing complexes have properties that make them potentially useful for imaging hypoxic vs normoxic environments and have been used to image tumors in vivo via direct injection.[3g] However, the critical limitation preventing Eu^{II}-containing complexes from imaging a wider range of hypoxia-containing conditions is their short-persistence time in normoxic environments that prevents both administration via systemic injection and imaging ratiometrically. Complexes **Eu1** and **Eu2**, reported here, have the ability to dissolve in the perfluorocarbon phase of emulsions that contain interfaces to slow O_2 transport in aqueous environments. Our preliminary reports demonstrate a persistence in vivo of the divalent oxidation state for a Eu-containing complex dispersed in a perfluorocarbon nanoemulsion on the order of tens of minutes, long enough to potentially enable systemic administration and ratiometric imaging. The perfluorocarbons in the emulsion are an enabling techology that provide ^{19}F signal that is scalable to the ratio of Eu^{II}/Eu^{III} and that provide support for the use of interfaces to slow the approach of O_2 into the outersphere environment of Eu^{II} dispersed within the nanoemulsions. Our investigations demonstrated a stark difference in signal between the oxidized and reduced forms of the complex, as well as an enlongated persistence of Eu^{II} in mice. The scalable intensity of the ^{19}F signal based on the proportion of Eu^{II} to Eu^{III} provides useful information for the creation of calibration curves based on pO_2 for measuring hypoxia in vitro. However, the need to know the concentration of Eu^{II} for a given signal intensity is a limitation of **Eu2** in vivo because changes in ^{19}F signal

intensity can occur from either the oxidation of Eu^{II} to Eu^{III} or the diffusion of **Eu1**/**Eu2** from a site of interest. The use of a second imaging modality for ratiometric imaging could overcome this limitation of concentration dependence of **Eu2** in vivo. This promising strategy is based on several other reported systems, for example, Gd^{III}-based contrast agents for MRI have been studied ratiometrically with positron emission tomography or near-IR fluorescent tags.[17] We are beginning to study such systems, and although no adverse events were observed in any of the mice post-injection, we plan to investigate toxicity of Eu^{II}-containing perfluorocarbons in the future. The results presented here are encouraging for the development of perfluorocarbon emulsion-based Eu agents for imaging hypoxic environments and are a major step toward overcoming the short persistance time of Eu^{II}-based contrast agents that prevent their use in a wide range of hypoxia-related diseases.

4. Experimental Section/Methods

Materials and Methods:

1H,1H-undecafluorohexylamine (97%); bromoacetylbromide (98%); potassium carbonate (98%); 1,4,7,10-tetraazacyclododecane (98%); europium(III) trifluoromethanesulfonate (98%); Eu-DOTA-4AmC; *n*-perfluorooctylbromide (98%); 1H,1H-perfluorooctylalcohol (98%); concentrated hydrochloric acid (ACS grade); activated neutral alumina powder (Brockmann I); anhydrous magnesium sulfate; phosphate-buffered saline (10×), CH_2Cl_2 (ACS grade); methanol (HPLC grade); and acetonitrile (ACS grade) were obtained from commercial sources and used as received. Deionized water was obtained from an ELGA PURELAB Ultra Mk2 water purification system with a resistivity of 18.0 Mω cm. {Europium(II) [(*N*,*N*′,*N*″,*N*‴-tetra(*N*-(4-trifluoromethylphenyl)acetamidyl)-1,4,7,10-tetraazacyclododecane]}bis-chloride was synthesized according to reported methods (**12F**).[18]

Physical Methods:

Elemental analysis was performed by Midwest Microlab (Indianapolis, IN). High resolution mass spectra were obtained using electrospray ionization on a Waters LCT premier time-of-flight HRMS in the Lumigen Instrument Center at Wayne State University. Sonication for the nanoemulsion preparation was performed using a Fisherbrand Model 50 Sonic Dismembrator.

NMR Spectroscopy:

NMR spectra for ^1H and^{19}F (except for Figure S19) were obtained using an Agilent MR (9.4 T), a Varian VNMRS (11.7 T), or a Bruker Advance NEO 500 MHz spectrometer in the Lumigen Instrument Center at Wayne State University. ^1H-NMR spectra were referenced to residual solvent peaks (δ = 7.26 for $HCCl_3$, δ = 2.50 ppm for dimethylsulfoxide (DMSO)) and ^{19}F-NMR were referenced to $CFCl_3$ (δ = 0.00 ppm) or trifluoromethanesulfonate anion (δ = 78.70 ppm). Multiplicities are described as m = multiplet, s = singlet, t = triplet, td = triplet of doublets, br = broad peak. The ^{19}F-NMR spectrum in Figure S18 was acquired on a 9.4 T Bruker AV NEO MRI with Paravision 360 software.

EPR Spectroscopy:

EPR spectra were acquired using a Bruker EMX X-band spectrometer with an Oxford variable-temperature cryostat in the Lumigen Instrument Center at Wayne State University. EPR samples were prepared in Wilmad Labglass 4 mm 707SQ250M tubes to a volume of 300 μL and sealed with paraffin wax under an atmosphere of N_2. Spectra were acquired in a degassed solution of 1H,1H-perfluorooctylalcohol/*n*-perfluorooctylbromide (20% *w*/*w*) at ambient temperature with a microwave frequency of 9.678654 GHz. Power was modulated for optimal signal.

Optical Spectroscopy:

UV–visible absorbance spectra were obtained using a Shimadzu UV mini-1240 spectrophotometer. Luminescence spectra were obtained using a HORIBA Jobin Yvon Fluoromax-4 spectrofluorometer. Solution-state samples in 1H,1H-perfluorooctylalcohol/*n*-perfluorooctylbromide (20% *w*/*w*) were placed in quartz cuvettes sealed using paraffin wax under an atmosphere of N_2. Absorbance-decay experiments were performed by exposing samples to the ambient atmosphere.

Particle Size Determination:

Particle size determination of the nanoemulsion was completed using a Spectradyne nCS1 particle size analyzer. Samples were prepared by diluting the prepared nanoemulsion described below by a factor of ten, and placing three microliters in a C-400 sample cartridge.

Magnetic Resonance Imaging:

All experimental protocols (AN-3334 and AN-6718) were approved by the institutional animal care and use committee (IACUC) at Baylor College of Medicine and were in accordance with the guidelines published in the National Institutes of Health Guide for Care and Use of Laboratory Animals.

Mouse imaging:

All MRI imaging was acquired using a 9.4 T Bruker AV NEO MRI with Paravision 360 software. Mice were induced with 5% isoflurane and transferred supine to the animal-imaging holder, and then transferred to the imaging instrument where 2% isoflurane was administered continuously via nose cone. A pressure-sensitive pillow was placed on the abdomen to constantly monitor respiration (Small Animal Instruments). The body temperature of the subject was also constantly monitored using a rectal probe and maintained at 37° using an air heater (Small Animal Instruments).

Intramuscular Injections:

Contrast agent (**Eu2**, 0.37 mM, 200 μL) was injected into the left thigh muscle of an anesthetized mouse while the mouse was on the imaging bed and just prior to imaging. The mouse was then placed within the magnet, and a localizer scan was acquired. Multiple ^{19}F-MRI (five time points) or T_1-weighted MRI scans (nine time points) were subsequently acquired.

^{19}F-MRI:

First, a single-pulse ^{19}F spectrum was acquired to monitor the presence of detectable ^{19}F signal. Next, ^{19}F-magnetic resonance chemical shift imaging was performed using a fast spin echo imaging sequence with the following imaging parameters: field of view = 32 mm × 32 mm; image size = 16 × 16 voxels, slice thickness = 15 mm; repetition time = 250 ms; echo time = 0.647 ms; number of averages = 8; 1024 FID data points; and spectral width = 25 kHz. Signal intensities were measured using Paravision 360 software.

T_1-weighted MRI:

A T_1-weighted RARE sequence was used for the T_1-weighted MRI scans with the following imaging parameters: TR = 504.000 ms, TE = 8.500 ms, a Rare Factor of 4, 1 repetition, 1 echo image, and 2 averages. Signal intensities were measured using Paravision 360 software.

Image Processing:

Color-coded figures for the ^{19}F-MRI phantoms were generated in Sivic. For the assessment of the T_1 signal, signal intensities were measured in Paravision 360 software and plotted using Prism Graphpad software. For the ^{19}F data, signal intensities were measured in PV 360 and then analyzed in Prism Graphpad software. The signal intensities were normalized to the initial time points for each animal.

Synthesis: N-(1H,1H-undecafluorohexyl)bromoacetamide:

1H,1H-Undecafluorohexylamine (912 μL, 5.00 mmol, 1 equiv) was dissolved in CH_2Cl_2 (15 mL). Potassium carbonate (1.5203 g, 11.000 mmol, 2.2 equiv) was suspended in this solution, and the mixture was cooled to 4 °C using an ice bath. Separately, bromoacetylbromide (481 μL, 5.5 mmol, 1.1 equiv) was dissolved in CH_2Cl_2 (2.5 mL). The solution of bromoacetylbromide was added to the cooled mixture of 1H,1H-undecafluorohexylamine dropwise over the course of 10 min. The resulting mixture was stirred for 30 min in an ice bath. The mixture was removed from the ice bath and stirred for an additional 30 min. Deionized water (7.5 mL) was added, and the mixture was stirred for 1 h. The aqueous and organic layers were separated, and the organic layer was washed with $HCl_{(aq)}$ (2 M, 2 × 5 mL). The organic layer was filtered through a plug of silica gel using CH_2Cl_2. The eluted solution was dried over $MgSO_4$. Solids were removed via filtration, and solvent was removed under reduced pressure to yield 1.76 g (84%) of a colorless powder. Elemental analysis of $C_8H_5NOF_{11}Br$ [mm = 420.02 g/mol] observed(calculated): %C 22.87(22.88); %H 1.23(1.20); %N 3.35(3.33). ESI-HRMS (methanol) of $C_8H_6NOF_{11}Br$ $[M + H]^+$ observed(calculated) m/z: 419.9450 (419.9452). ^{1}H-NMR ($CDCl_3$, ppm): 6.79 (s, 1H), 4.05 (td, 2H), 3.96 (s, 2H). ^{19}F-NMR ($CDCl_3$, ppm): −80.80 (t, 3F), −118.00 to −118.35 (m, 2F), −122.65 to −122.97 (m, 2F), −123.42 to −123.67 (m, 2F), −126.12 to −126.43 (m, 2F).

N,N',N",N"'-tetra(N-(1H,1H-undecafluorohexyl)acetamidyl)-1,4,7,10-tetraazacyclododecane:

In acetonitrile (20 mL) was dissolved N-(1H,1H-undecafluorohexyl)bromoacetamide (0.9450 g, 2.250 mmol, 4.5 equiv) and 1,4,7,10-tetraazacyclododecane (0.0861 g, 0.500 mmol, 1 equiv). Potassium carbonate (0.5183 g, 3.750 mmol, 7.5 equiv) was added to the

solution, and the resulting mixture was stirred at 65 °C for 72 h. The mixture was vacuum filtered using a water aspirator, and the filtrate was concentrated to an orange powder under reduced pressure. The crude product was purified using flash column chromatography (neutral alumina, methanol/CH_2Cl_2 gradient from 2 to 10%) to obtain an off-white powder. The powder was triturated (7.5 mL of refluxing acetonitrile) then vacuum filtered while hot using a water aspirator to yield 684 mg (84%) of the final product as a potassium complex bicarbonate salt as a colorless powder. Elemental analysis of $C_{41}H_{37}N_8O_7F_{44}K$ [mm = 1628.82 g/mol] observed(calculated): %C 30.15(30.23); %H 2.28(2.29); %N 6.90(6.88). ESI-HRMS (methanol) of $C_{40}H_{37}N_8O_4F_{44}$ $[M + H]^+$ observed(calculated) *m*/*z*: 1529.2255(1529.2230). ^{1}H-NMR (DMSO-d_6, ppm): 8.66 (t, 4H) 4.01 to 3.85 (m, 8H), 3.32 (br, 8H, overlaps with H_2O), 3.09 (br, 8H), 2.23 (br, 8H). ^{19}F-NMR (DMSO-d_6, ppm): −81.13 (br, 12F), −118.04 (br, 8F), −123.19 (br, 8F), −123.89 (br, 8F), −126.64 (br, 8F).

{Europium(III) [(N,N',N",N"'-tetra(N-(1H,1H-undecafluorohexyl)acetamidyl)-1,4,7,10-tetraazacyclododecane]}tris(trifluoromethanesulfonate) tetrahydrate (Eu1):

N,*N*',*N*",*N*"'-Tetra(N-(1H,1H-undecafluorohexyl)acetamidyl)-1,4,7,10-tetraazacyclododecane (0.7644 g, 0.5000 mmol, 1 equiv) and europium(III) trifluoromethanesulfonate (0.2996 g, 0.5000 mmol, 1 equiv) were dissolved in a mixture of acetonitrile (12.5 mL) and methanol (2.5 mL). The solution was warmed to 60 °C and stirred for 24 h. Then the solution was vacuum filtered using a water aspirator and washed with cold (4 °C) acetonitrile (2 × 5 mL). The filtrate was condensed under reduced pressured to yield 1.045 g (95%) of a colorless solid. Elemental analysis of $EuC_{43}H_{44}N_8O_{17}F_{53}S_3$ [mm = 2199.92 g/mol] observed(calculated): %C 23.39(23.48); %H 1.82(2.02); %N 4.92(5.09). ESI-HRMS (methanol) of $EuC_{40}H_{36}N_8O_4F_{44}$ $[M]^{3+}$ observed(calculated) *m*/*z*: 560.3781(560.3784). ^{1}H-NMR (DMSO-d_6, ppm): 12.91 (br), 5.04 (br), 3.93 (br), 3.03 (br), −0.50 (br), −3.34 (br), −5.06 (br), −8.53 (br). ^{19}F-NMR (DMSO-d_6, ppm): −81.46 (br), −118.80 (br), −123.76 (br), −124.34 (br), −127.13 (br).

Reduction procedure for europium(II) complex (Eu2):

The following procedure was performed under an atmosphere of N_2 using a wet glovebox (no O_2 but water allowed). {Europium(III)[(N,N',N",N"'-tetra(N-(1H,1H-undecafluorohexyl)acetamidyl)-1,4,7,10-tetraazacyclododecane]}tris(trifluoromethanesulfonate) (10 mg, 4.5 μmol) was dissolved in degassed 1H,1H-perfluorooctylalcohol/*n*-perfluorooctylbromide (20% *w*/*w*, 1 mL). Zinc dust (150 mg, 2.29 mmol) was added to the resulting solution, and the mixture was stirred at ambient temperature for 24 h. The resulting yellow solution was filtered using 20 μm Teflon syringe filters. EPR and UV–visible spectroscopies confirmed the reduction of Eu^{III} to Eu^{II}. ^{1}H-NMR in DMSO-d_6 only shows residual solvent peaks, and ^{19}F-NMR shows weak signal from the fluorinated tetra-amide complex. ^{19}F-NMR (DMSO-d_6, ppm): −81.59 (br), −82.00 (br), −119.06 (br), −123.81 (br), −124.22 (br), −124.46 (br), −125.17 (br), −127.21 (br), −127.59 (br).

Complex-loaded perfluorocarbon nanoemulsion preparation:

The following procedure was performed under an atmosphere of N_2 using a wet glovebox (no O_2 but water allowed). Lecithin (250 mg) was suspended in phosphate-buffered saline

(1x, 5 mL) and allowed to sit for 30 min. The resulting suspension was warmed to 80 °C and stirred vigorously for 1 h. To the warm suspension was added a solution of **Eu1** or **Eu2** (~4.5 mM) in degassed 1H,1H-perfluorooctylalcohol/*n*-perfluorooctylbromide (500 μL, 20% *w*/*w*). The resulting suspension was stirred for 1 h at which point heat was removed and stirring was continued for 1 h. The cooled suspension was sonicated using a sonic dismembrator operated at 25% power by cycling 20 s on followed by 20 s off for a total period of 20 min. The nanoemulsions were characterized to have an average particle size of 199 ± 31 nm. ^{19}F-NMR (ppm) of either **Eu1**- or **Eu2**-containing emulsion in phosphate-buffered saline (1x) (10% v/v D_2O) have peaks at −65.25 (t), −83.27 (t), −118.96 (br), −122.61 (br), −123.41 (br), −124.32 (br), −125.15 (br), and −128.02 (br)

Statistical Analysis—Statistical significiance for ^{19}F signal intensities between C and D (n = 3) in ^{19}F-magnetic resonance chemical shift imaging was calculated using Microsoft Excel software with a two-sided unpaired *t*-test. Standard error of the mean for in vivo ^{1}H- and ^{19}F-MRI represents the sample standard deviation divided by the square root of sample size.

Supplementary Material

Refer to Web version on PubMed Central for supplementary material.

Acknowledgements

JCL and ALB contributed equally to this work. The authors gratefully acknowledge funding from the National Institutes of Health (R01EB026453 and R01EB027103). AGS was supported by the National Institutes of Health (T32 GM142519). The NMR laboratory is partially supported by the NIH (S10OD028488). The authors are grateful to Prof. Tom Linz and Ms. Bailey Riley for their help with particle size determination using a Spectradyne nCS1 Particle Size Analyzer. The authors also gratefully acknowledge the use of the Small Animal Imaging Facility (SAIF) at Texas Children's Hospital.

References

[1]. a)Semenza GL, Cancer Metastasis Rev. 2007, 26, 223–224; [PubMed: 17404692] b)Wilson WR, Hay MP, Nat. Rev. Cancer 2011, 11, 393–410; [PubMed: 21606941] c)Schito L, Semenza GL, Trends Cancer 2016, 2, 758–770; [PubMed: 28741521] d)Bexell D, Pharmacol. Ther 2016, 164, 152–169; [PubMed: 27139518] e)Jing X, Yang F, Shao C, Wei K, Xie M, Shen H, Shu Y, Mol. Cancer 2019, 18, 157. [PubMed: 31711497]

[2]. a)Keeley TP, Mann GE, Physiol. Rev 2019, 99, 161–234; [PubMed: 30354965] b)Papkovsky DB, Dmitriev RI, Cell. Mol. Life Sci 2018, 75, 2963–2980; [PubMed: 29761206] c)Lee AL, Gee CT, Weegman BP, Einstein SA, Juelfs AR, Ring HL, Hurley KR, Egger SM, Swindlehurst G, Garwood M, Pomerantz WCK, Haynes CL, ACS Nano 2017, 11, 5623–5632; [PubMed: 28505422] d)Yu D, Yang J, Wang L, Chen M, Yang R, Zheng J, Chem. Commun 2022, 58, 3661–3664;e)He M, Zhong Z, Zeng D, Gong X, Wang Z, Li F, Biomed. Eng. Online 2021, 20, 91; [PubMed: 34526014] f)Lawrence DJ, Escott ME, Myers L, Intapad S, Lindsey SH, Bayer CL, Sci. Rep 2019, 9, 558; [PubMed: 30679723] g)Spanoudaki V, Doloff J, Huang W, Norcross SR, Farah S, Langer R, Anderson DG, Proc. Natl. Acad. Sci. U.S.A 2019, 116, 4861–4870; [PubMed: 30808810] h)Guan Y; Niu H; Dang Y; Gao N; Guan J Acta Biomater. 2020, 115, 333–342. [PubMed: 32853800]

[3]. a)Srivastava K, Weitz EA, Peterson KL, Marjanska M, Pierre VC, Inorg. Chem 2017, 56, 1546–1557; [PubMed: 28094930] b)Kadakia RT, Xie D, Guo H, Bouley B, Yu M, Que EL, Dalton Trans. 2020, 2, 1–19;c)Wang H, Jordan VC, Ramsay IA, Sojoodi M, Fuchs BC, Tanabe KK, Caravan P, Gale EM, J. Am. Chem. Soc 2019, 141, 5916–5925; [PubMed: 30874437] d)Xie D,

Yu M, Kadakia RT, Que EL, Acc. Chem. Res 2020, 53, 2–10; [PubMed: 31809009] e)Xie D, Kim S, Kohli V, Banerjee A, Yu M, Enriquez JS, Luci JJ, Que EL, Inorg. Chem 2017, 56, 6429–6437; [PubMed: 28537705] f)Xie D, King TL, Banerjee A, Kohli V, Que EL, J. Am. Chem. Soc 2016, 138, 2937–2940; [PubMed: 26906216] g)Ekanger LA, Polin LA, Shen Y, Haacke EM, Martin PD, Allen MJ, Angew. Chem. Int. Ed 2015, 54, 14398–14401;h)Ekanger LA, Polin LA, Shen Y, Haacke EM, Martin PD, Allen MJ, Angew. Chem 2015, 127, 14606–14609;i)Tsitovich PB, Burns PJ, McKay AM, Morrow JR, J. Inorg. Biochem 2014, 133, 143–154. [PubMed: 24529651]

[4]. A Ekanger L, Basal LA, Allen MJ, Chem. Eur. J 2017, 23, 1145–1150. [PubMed: 27897355]

[5]. a)Ekanger LA, Mills DR, Ali MM, Polin LA, Shen Y, Haacke EM, Allen MJ, Inorg. Chem 2016, 55, 9981–9988; [PubMed: 27244124] b)Lenora CU, Carniato F, Shen Y, Latif Z, Haacke EM, Martin PD, Botta M, Allen MJ, Chem. Eur. J 2017, 23, 15404–15414. [PubMed: 28707809]

[6]. a)Basal LA, Bailey MD, Romero J, Ali MM, Kurenbekova L, Yustein J, Pautler RG, Allen MJ, Chem. Sci 2017, 8, 8345–8350; [PubMed: 29780447] b)Ekanger LA, Polin LA, Shen Y, Haacke EM, Allen MJ, Contrast Media Mol. Imaging 2016, 11, 299–303. [PubMed: 27028559]

[7]. a)Yee EL, Gansow OA, Weaver MJ, J. Am. Chem. Soc 1980, 102, 2278–2285;b)Burai L, Tóth É, Moreau G, Sour A, Scopelliti R, Chem. Eur. J 2003, 9, 1394–1404; [PubMed: 12645029] c)Gansow OA, Kausar AR, Triplett KM, Weaver MJ, Yee EL, J. Am. Chem. Soc 1977, 99, 7087–7089;d)Gamage NH, Mei Y, Garcia J, Allen MJ, Angew. Chem. Int. Ed 2010, 49, 8923–8925;e)Gamage NH, Mei Y, Garcia J, Allen MJ, Angew. Chem 2010, 122, 9107–9109.

[8]. Ekanger LA, Allen MJ, Metallomics 2015, 7, 405–421. [PubMed: 25579206]

[9]. Ekanger LA, Ali MM, Allen MJ, Chem. Commun 2014, 50, 14835–14838.

[10]. Rashid MM, Corbin BA, Jella P, Ortiz CJ, Samee MAH, Pautler RG, Allen MJ, J. Am. Chem. Soc, accepted, DOI: 10.1021/jacs.2c10373

[11]. a)Kim S, Kim S, Oh WY, Lee Y, Lee J, Int. J. Food Sci 2022, 57, 6082–6089;b)Kimmich R, Peters A, Spohn KH, J. Membr. Sci 1981, 9, 313–336.

[12]. a)Riess JG, Krafft MP, Biomaterials; 1998, 19, 1529–1539; [PubMed: 9794531] b)Krafft MP, J. Fluor. Chem 2015, 177, 19–28;c)Krafft MP, Chittofrati A, Reiss JG, Curr. Opin. Colloid Interface Sci 2003, 8, 251–258;d)Huang MQ, Ye Q, Williams DS, Ho C, Magn. Reson. Med 2002, 48, 487–492; [PubMed: 12210913] e)Mason RP, Antich PP, Babcock EE, Gerberich JL, Nunnally RL, Magn. Reson. Imaging 1989, 7, 475–485; [PubMed: 2607898] f)Patel SK, Williams J, Janjic JM, Biosensors 2013, 3, 341–359; [PubMed: 25586263] g)Riess JG, Artif. Cells Blood Substit. Immobil. Biotechnol 2005, 33, 47–63; [PubMed: 15768565] h)Zhuang J, Ying M, Spiekermann K, Holay M, Zhang Y, Chen F, Gong H, Lee JH, Gao W, Fang RH, Zhang L, Adv. Mater 2018, 30, 1804693.i)Grote J, Steuer K, Müller R, Söntgerath C, Zimmer K, Adv. Ex. Med. Biol 1985, 453–461;j)Clark LC, Gollan F, Science 1966, 152, 1755–1756 [PubMed: 5938414]

[13]. Patrick MJ, Janjic JM, Teng H, O'Hear MR, Brown CW, Stokum JA, Schmidt BF, Ahrens ET, Waggoner AS, J. Am. Chem. Soc 2013, 135, 18445–18457; [PubMed: 24266634] b)Kislukhin AA, Xu H, Adams SR, Narsinh KH, Tsien RY, Ahrens ET, Nat. Mater 2016, 15, 662–668. [PubMed: 26974409]

[14]. a)Subasinghe SAAS, Romero J, Ward CL, Bailey MD, R Zehner D, Mehta PJ, Carniato F, Botta M, Yustein JT, Pautler RG, Allen MJ, Chem. Commun 2021, 57, 1770–1773;b)Basal LA, Yan Y, Shen Y, Haacke EM, Mehrmohammadi M, Allen MJ, ACS Omega 2017, 2, 800–805. [PubMed: 28393130]

[15]. a)Jahanvi V, Kelkar A, S. Afr. J. Rad 2021, 25, a2061;b)Brink HF, Buschmann MD, Rosen BR, Comput. Med. Imaging Graph 1989, 13, 93–104. [PubMed: 2538222]

[16]. Sherry AD, Caravan P, Lenkinski RE, J. Magn. Reson. Imaging 2009, 30, 1240–1248. [PubMed: 19938036]

[17]. a)Frullano L, Catana C, Brenner T, Sherry AD, Caravan P, Angew. Chem. Int. Ed 2010, 76, 6463–6470;b)Flögel U, Temme S, Jacoby C, Oerther T, Keul P, Flocke V, Wang X, Bönner F, Nienhaus F, Peter K, Schrader J, Grandoch M, Kelm M, Levkau B, Nature Comm. 2021, 12, 5847;c)Song Y, Zong H, Trivedi ER, Vesper BJ, Waters EA, Barrett AGM, Radosevich JA, Hoffman BM, Meade TJ, Bioconjugate Chem. 2021, 21, 2267–2275.d)Subasinghe SAAS, Pautler RG, Samee MAH, Yustein JT, Allen MJ, Biosensors, 2022, 12, 478. [PubMed: 35884281]

[18]. Subasinghe SAAS, Romero J, Ward CL, Bailey MD, Zehner DR, Mehta PJ, Carniato F, Botta M, Yustein JT, Pautler RG, Allen MJ, Chem. Commun 2021, 57, 1770–1773.

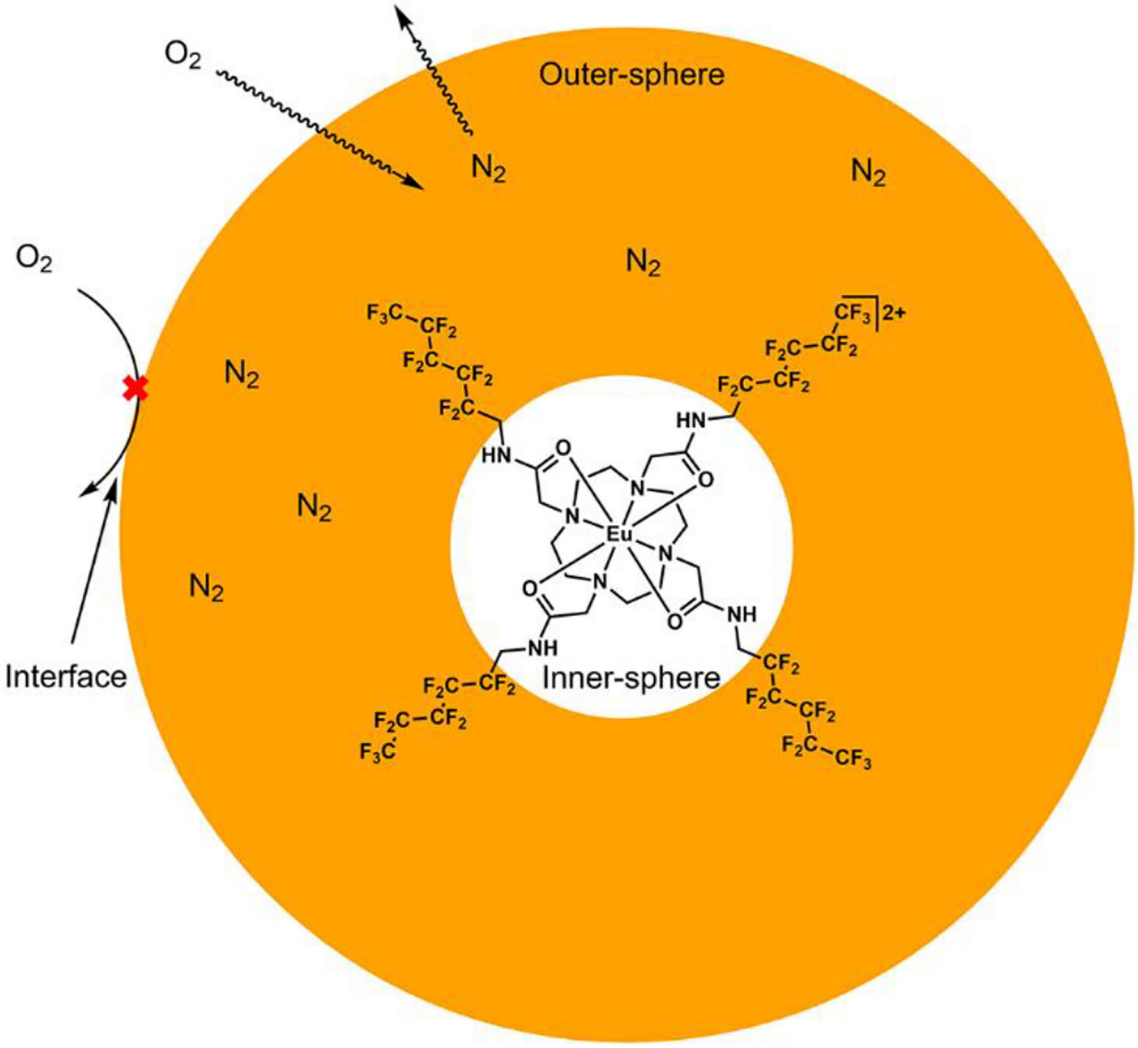

Figure 1.

Cartoon representation of a perfluorocarbon nanoemulsion hindering the approach of oxygen into the outersphere of **Eu2** (**Eu1** is the same complex but with Eu^{III} instead of Eu^{II}). Orange color represents the perfluorocarbon that is also the outersphere environment of dispersed Eu^{II}. The white color at the center representes the innersphere of Eu^{II}. The perfluorocarbon is degassed to removed O_2 then saturated with N_2 by exposure in a glovebox. The outer edge of the orange circle represents two interfaces (perfluorocarbon/ lecithin and lecithin/water) that slow diffusion of O_2 into the perfluorocarbon (outersphere of Eu^{II}), thus increasing the persistance time of Eu^{II} before oxidation to Eu^{III} relative to systems without multiple interfaces. ^{19}F-MRI signal from the perfluorocarbon is small in the presence of Eu^{II} and large in the presence of Eu^{III}. Only one complex of Eu^{II} is shown for clarity.

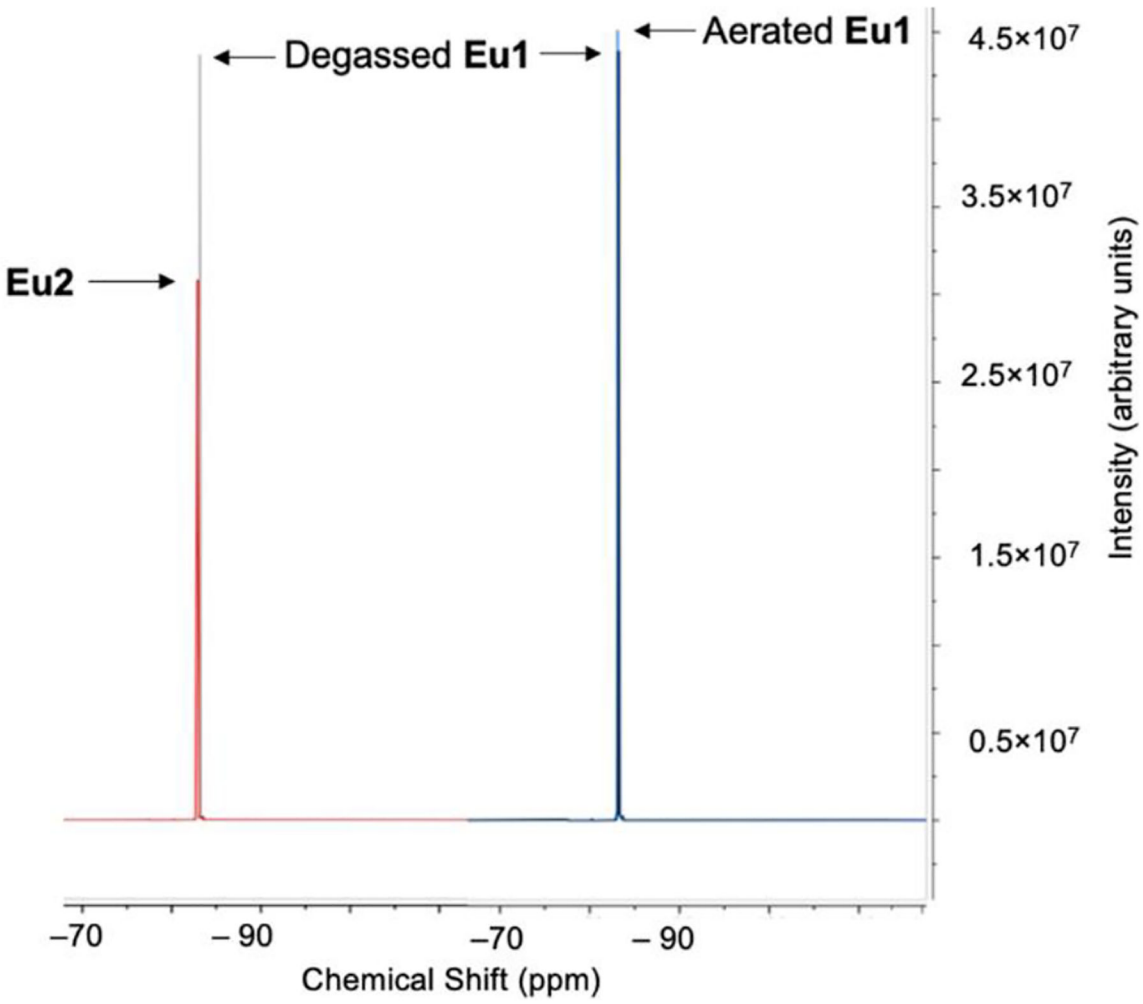

Figure 2.

(Left) Overlay of ^{19}F-NMR spectra of **Eu1** (4.5 mM) and **Eu2** (4.5 mM) in degassed N-perfluorooctylbromide (80%) and 1H,1H-perfluorooctylalcohol (20%). (Right) Overlay of ^{19}F-NMR spectra of degassed **Eu1** and aerated **Eu1**. The difference in peak intensity on the left (Degassed **Eu1** minus **Eu2**) is more than an order of magnitude larger than the difference on the right (Aerated **Eu1** minus Degassed **Eu1**), demonstrating that Eu oxidation, and not the presence of oxygen, is the primary factor responsible for ^{19}F signal change. See supporting information for full difference spectra.

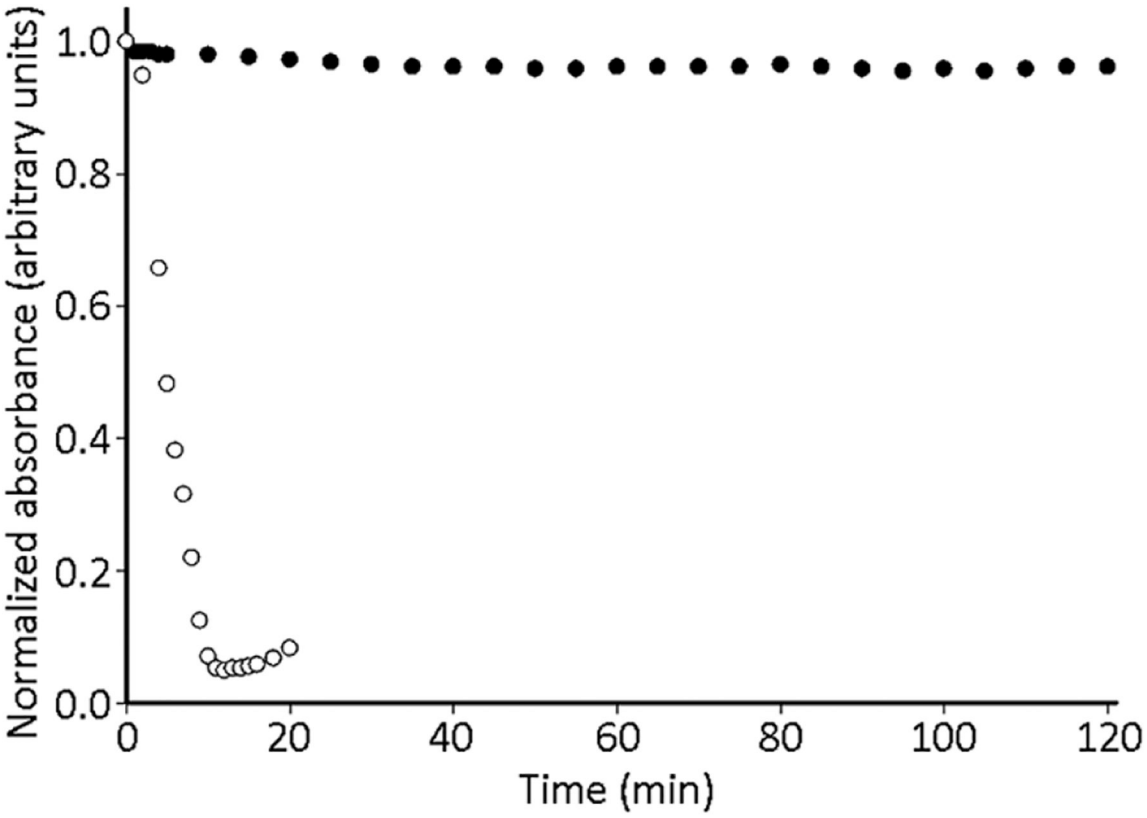

Figure 3.

Timecourse UV–visible absorbance for **Eu2** (0.37 mM) in 20% (*w*/*w*) PFOA in PFOB (○) and the Eu2 solution with a layer of 500 μL of nondegassed water to create an extra interface (●). Both sets of data monitored 350 nm.

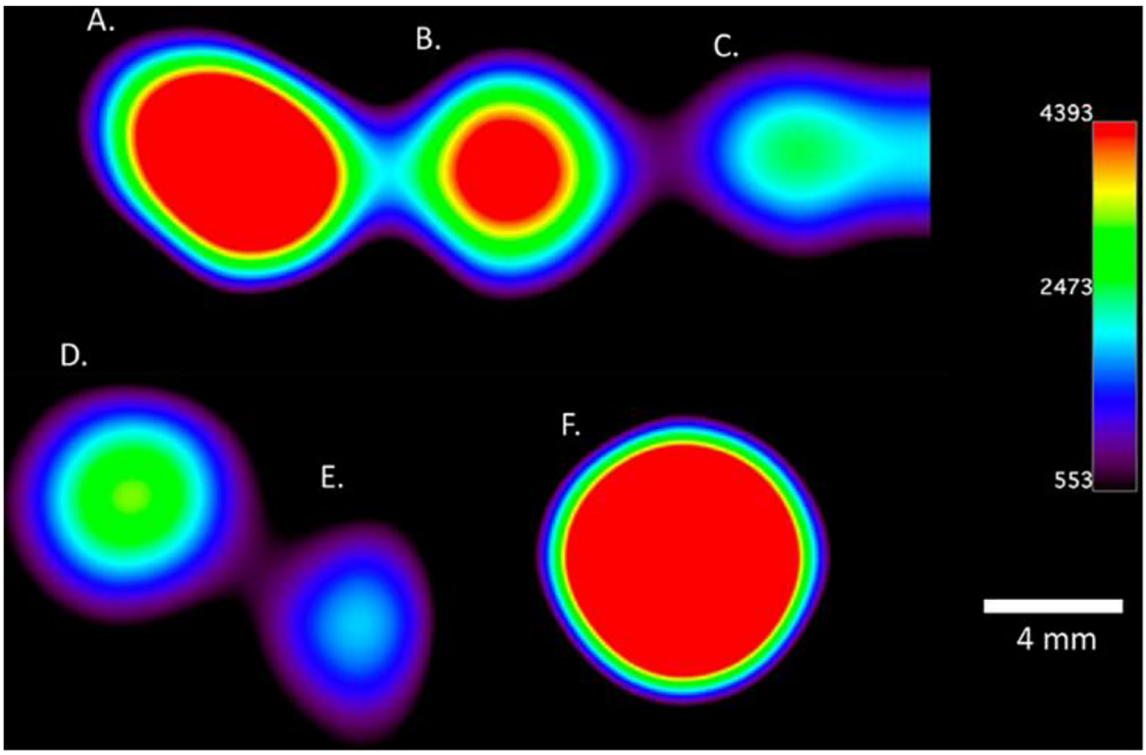

Figure 4.

Chemical-shift imaging of emulsions prepared in the absence of O_2 that contain controlled mixtures of **Eu1**/**Eu2**: A. 0% **Eu2**, B. 25% **Eu2**, C. 50% **Eu**2, D. 75% **Eu2**, E. 100% **Eu2**, and F. trifluoroacetic acid as a reference. All samples contained a total concentration of Eu of 0.37 mM and perfluorocarbons of 0.28 M. Imaging was performed at 9.4 T with an acquisition time of 8 min 32 s.

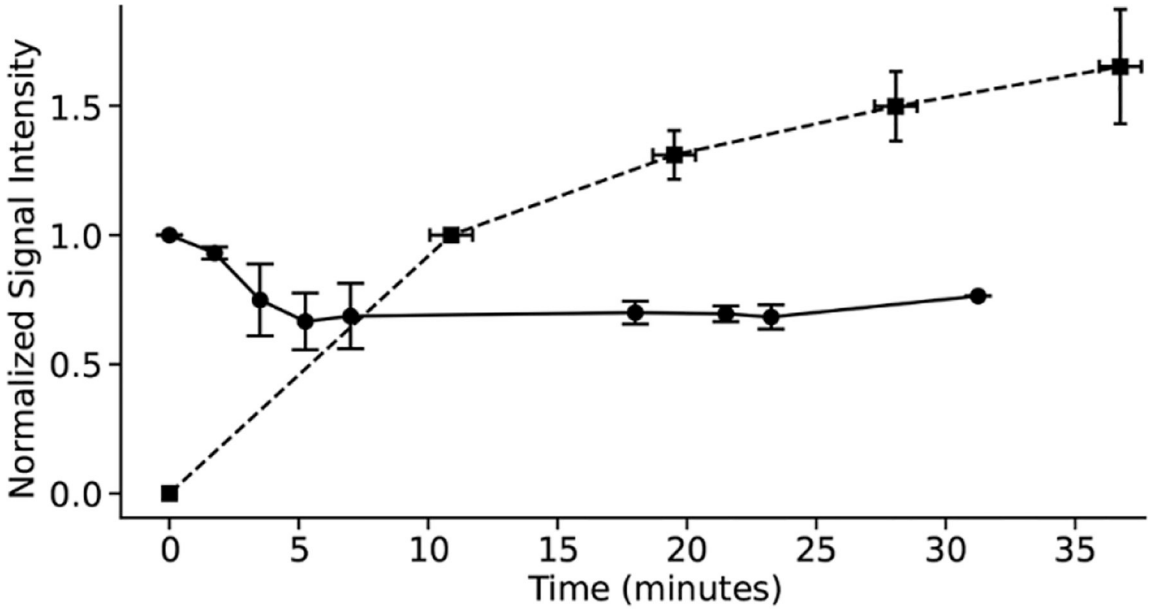

Figure 5.

In vivo measurements of ^{1}H-MRI signal for **12F** (●) and ^{19}F-MRI signal intensity for **Eu2** (■). The decrease in signal intensity of ^{1}H-MRI signifies oxidation of Eu^{II} in **12F**, and the increase in ^{19}F-MRI signal intensity signifies oxidation of Eu^{II} in **Eu2**. Initial signal intensities are normalized to 1.0 for the initial ^{1}H-MRI signal and 0.0 for the initial ^{19}F-CSI. Error bars represent the standard error of the mean of three different mice, and lines are guides for the eyes.